



# Ignition and combustion of Perfluoroalkyl-functionalized aluminum nanoparticles and nanothermite

Yue Jiang<sup>a</sup>, Yujie Wang<sup>b</sup>, Jihyun Baek<sup>a</sup>, Haiyang Wang<sup>b</sup>, Jennifer L. Gottfried<sup>c</sup>,  
Chi-Chin Wu<sup>c</sup>, Xinjian Shi<sup>a</sup>, Michael R. Zachariah<sup>b,\*</sup>, Xiaolin Zheng<sup>a,\*</sup>

<sup>a</sup> Department of Mechanical Engineering, Stanford University, Stanford, CA 94305, USA

<sup>b</sup> Department of Chemical and Environmental Engineering, University of California, Riverside, CA 92521, USA

<sup>c</sup> Weapons and Materials Research Directorate, US Army Combat Capabilities Development Command Army Research Laboratory, Aberdeen Proving Ground, Aberdeen, MD 21005, USA



## ARTICLE INFO

### Article history:

Received 14 January 2022

Revised 15 April 2022

Accepted 18 April 2022

Available online 2 May 2022

### Keywords:

Energetic materials  
Aluminum combustion  
Functionalization  
Perfluoroalkylsilane  
Thermite

## ABSTRACT

Aluminum (Al) is an excellent metal fuel for combustion applications because of its high energy density and low cost. Nano-sized Al (nAl) particles have relatively low ignition temperature and high reactivity, but their performance is limited by the presence of the native oxide ( $\text{Al}_2\text{O}_3$ ) layer surrounding the active Al core. To overcome this problem, nAl coated or mixed with fluorocarbon species have been intensively studied recently. In this work, we demonstrate a facile method to functionalize the surface of nAl particles with perfluoroalkylsilane and investigate the thermochemical and combustion behaviors of perfluoroalkyl-functionalized nAl particles at both slow and fast heating rates. At slow heating rates, the covalently-bonded perfluoroalkylsilane molecules partially undergo debonding at low temperatures before reacting with  $\text{Al}_2\text{O}_3$ . The remaining perfluoroalkyl molecules slowly react with surface oxide to thicken the surface shell, which improves the thermal stability of nAl particles. Nevertheless, under fast heating conditions, the dissociated fluorine species can readily react with the oxide on the nAl surface, enhancing the ignition and combustion performance of both nAl particles in the air and Al/copper (II) oxide (CuO) nanothermite. These results advance the understanding of the thermochemical behaviors of the fluorocarbon species and their effects on the ignition and combustion of nAl particles and Al-based energetic materials.

© 2022 The Combustion Institute. Published by Elsevier Inc. All rights reserved.

## 1. Introduction

Metal fuels are essential for energetic applications that require high energy densities, ranging from power generation, materials synthesis and processing, aviation, to space propulsion [1–6]. Aluminum (Al) is the most commonly used metal fuel because of its high energy density, earth abundance, and low cost [7]. The ignition and combustion properties of Al are known to be size-dependent [8]. In comparison to micron-sized Al ( $\mu\text{Al}$ ) particles, the nano-sized Al (nAl) particles have a much higher specific surface area, a reduced diffusion distance, leading to a higher reactivity and a lower ignition temperature [6,9,10]. However, a critical challenge of nAl is its high content of the native oxide ( $\text{Al}_2\text{O}_3$ ) layer (2–5 nm) [11,12]. The presence of a native oxide shell not only reduces the active Al content and energy density of nAl but also

slows down the mass transport through the oxide layer [13,14]. The presence of oxide shell also inhibits the oxidation of  $\mu\text{Al}$ , so the ignition temperature of  $\mu\text{Al}$  is close to the melting point of  $\text{Al}_2\text{O}_3$  [10,15].

To overcome the native oxide problem, various methods have been explored to modify the surface structure and/or the composition of Al. The most straightforward approach is to remove the native oxide shell or synthesize oxide-free Al particles and then form a passivation layer consisting of other materials that can react with Al, including metals (e.g., nickel) [16] and fluorocarbons (e.g., fluorocarboxylic acid, polyvinylidene fluoride) [17–19]. This strategy could effectively increase the reactivity and reduce the ignition threshold of Al-based energetic materials. It should be noted that the oxide-free Al particles are highly reactive and potentially dangerous. An alternative approach is to functionalize the native oxide to make it reactive in its own right. For this approach, fluorine-containing species have been often adopted. First, the fluorination of Al has a higher combustion enthalpy than the Al oxidation [12,20,21]. Second, a pre-ignition reaction occurs between the fluorine species and  $\text{Al}_2\text{O}_3$  so that the inner Al core

\* Corresponding authors.

E-mail addresses: [mrz@engr.ucr.edu](mailto:mrz@engr.ucr.edu) (M.R. Zachariah), [xlzheng@stanford.edu](mailto:xlzheng@stanford.edu) (X. Zheng).

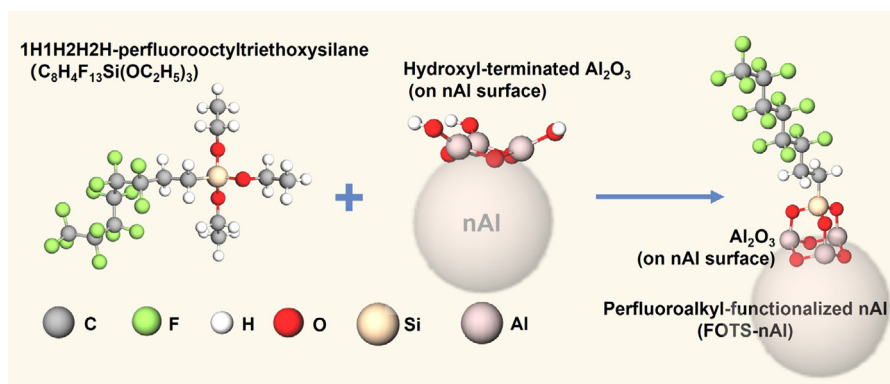


Fig. 1. Schematic illustration of the molecular structure of  $C_8H_4F_{13}Si(OC_2H_5)_3$  (FOTS) and the functionalization process of nAl to FOTS-nAl.

can be more easily exposed to the oxidizer [22]. Moreover, the combustion product aluminum fluoride ( $AlF_3$ ) is more volatile than  $Al_2O_3$  at elevated temperatures, which can help to reduce the agglomeration of condensed phase products and enhance combustion efficiency [23–25]. Previous works have shown that coating nAl with fluorocarbons simultaneously promotes its reactivity and stability [26–28]. However, many of those coatings involve physically adsorbed fluorocarbons. It is of interest to study nAl particles that are only covalently functionalized with fluorocarbons and have a low-content fluorocarbon functionalization, which may lessen the undesired reduction in energy density. Moreover, it is necessary to investigate the thermochemical and oxidation behaviors of fluorocarbon-functionalized nAl under different heating rates.

Herein, we functionalized nAl particles with perfluoroalkylsilane molecules via a facile and ambient-condition synthetic method. Perfluoroalkylsilane was chosen as it can react with the hydroxyl group on the nAl surface to form covalent bonds under ambient conditions, and it is commercially available, which facilitates the scale-up sample preparation and applications. The thermochemical behavior of functionalized nAl particles and nAl/CuO nanothermite was investigated by thermogravimetric analysis (TGA) and differential scanning calorimetry (DSC) at a slow heating rate ( $10\text{ }^\circ\text{C}/\text{min}$ ). The ignition and combustion of nAl and nAl/CuO nanothermite were studied at much higher heating rates –  $10^5$ – $10^6\text{ }^\circ\text{C}/\text{s}$  via T-jump and flash ignition techniques and/or  $10^{13}\text{ }^\circ\text{C}/\text{s}$  via the laser-induced air shock from energetic materials (LASEM) method. We found that perfluoroalkyl-functionalized nAl exhibits a delayed onset temperature for slow oxidation, implying that the perfluoroalkylsilane functionalization improves the thermal stability of nAl particles. The nanothermite with perfluoroalkyl-functionalized nAl has a similar onset temperature of reaction during slow heating as the one with pristine nAl. In contrast, under fast heating conditions, perfluoroalkyl-functionalized nAl and its nanothermite show a reduced ignition threshold and an enhanced reactivity. Our analysis of the combustion products reveals that the perfluoroalkyl surface functionalization effectively removes or breaks the oxide shell with less agglomerated products, especially under fast heating rates. Those results suggest that nAl with a low content of perfluoroalkyl-functionalization has enhanced thermal stability and better reactivity, beneficial for many combustion applications.

## 2. Experimental specifications

### 2.1. Materials preparation

The nAl particles (nominal diameter of 70 nm, US Nano, ~72.5 wt% of active content) were functionalized with 1H,1H,2H,2H-perfluorooctyltriethoxysilane ( $C_8H_4F_{13}Si(OC_2H_5)_3$ ), known as FOTS,

98%, Sigma-Aldrich) using the silylation chemistry (Fig. 1), a method that we have used to functionalize boron previously [29]. Briefly, 100 mg of nAl particles were first dispersed in 10 ml of dichloromethane (DCM, 99.9%, ACROS Organics) and sonicated for 30 min. 0.5 ml of FOTS was subsequently added into the nAl/DCM suspension dropwise and the suspension was vigorously stirred for 8 h. The resulting functionalized nAl (FOTS-nAl) particles were centrifuged and washed with DCM three times to remove the residual unbound FOTS. The collected powders were further dried in a desiccator to remove the residual solvent. For the preparation of nAl/CuO thermite samples, nAl and CuO (50 nm in diameter, Sigma-Aldrich) powders were physically mixed and sonicated in hexane for 30 min. The equivalence ratio between nAl and CuO was kept as 1.0 while considering only the active Al mass in pristine and functionalized nAl particles (not including oxides and functionalization layers). The same synthetic procedure was also used to prepare  $\mu\text{Al}$  and  $\mu\text{Al}/\text{CuO}$  thermite samples for comparison.

### 2.2. Materials characterization

The morphology and elemental composition of the pristine and functionalized Al particles and their combustion products were characterized by scanning electron microscopy (SEM, FEI Magellan 400) with energy-dispersive X-ray spectroscopy (EDXS). The detailed surface morphology of Al particles was observed by transmission electron microscopy (TEM) utilizing a JEOL JEM 2100F with 200 kV accelerating voltage. The surface composition of the functionalized nAl particles at elevated temperatures was investigated via X-ray photoelectron spectroscopy (XPS, PHI VersaProbe) with the CasaXPS software.

### 2.3. TGA/DSC measurements

The thermochemical behavior of pristine and functionalized nAl particles was investigated by simultaneous TGA/DSC (Setaram Lab-sys Evo). For each measurement, 5 mg of the sample powders were placed in a 100  $\mu\text{l}$  alumina crucible, which was then heated in the TGA/DSC chamber from room temperature to  $1000\text{ }^\circ\text{C}$  at a heating rate of  $10\text{ }^\circ\text{C}/\text{min}$  with an airflow of 40 standard cubic centimeters per minute (sccm). After cooling down to room temperature, the sample was reheated with the same process, and the reheating curve was used to correct the baseline of the first heating process. The integrated peak area of DSC curves indicates the heat release of the specific exothermic peak. Similar DSC experiments were also conducted for pristine and functionalized nAl/CuO thermites using the same heating profile but in a 40 sccm argon flow.

## 2.4. T-Jump ignition experiments

Perfluoroalkyl-functionalized nAl particles and their thermite with CuO were analyzed with temperature-jump ignition (T-Jump ignition), a technique described in detail in previous work [30]. The sample was first dispersed in hexane and sonicated for 30 min and then coated on a Pt wire (76  $\mu\text{m}$  in diameter). The loaded Pt wire was inserted into a chamber filled with air and rapidly joule-heated to  $\sim 1000$  °C by a 3 ms pulse. The temporal voltage and current of the wire were recorded during heating and the instantaneous temperature was calculated based on the Callendar-Van Dusen equation. A Vision Research Phantom v12.0 high-speed camera with a high frame rate was used to determine the ignition event on the wire.

## 2.5. Flash ignition and time-resolved pressure measurement

The experimental setup for the flash ignition and the time-resolved pressure measurement in a constant-volume vial have been described in our previous works [12,31]. For a typical experiment of flash ignition in the open air, either 10 mg of pristine or functionalized nAl sample or 5 mg of pristine or functionalized nAl/CuO thermite sample was placed on a 1-mm thick glass slide on top of the Xe ring tube of a commercial flash unit (AlienBees B1600). All the samples were packed to have a porosity of  $\sim 85\%$ . A high-speed camera (Photron FASTCAM SA5) was used to capture the burning process of flash-ignited samples at 5200 frames per second (fps). A high-speed infrared (IR) camera (FLIR X6900sc) was used to quantify the temperature dynamics of samples after flash ignition at 1000 fps. For the time-resolved pressure measurement, 10 mg of powders were loaded in a 20 ml glass vial in air, and the vial with the sample was placed on top of the Xe flash ring tube and then ignited by the Xe flash lamp at a power of 2.1 J/cm<sup>2</sup>. The pressure history from reactions was recorded by a pressure transducer (603B1, Kistler Inc.).

## 2.6. LASEM measurement

The experimental setup for the laser-induced air shock from energetic materials (LASEM) was described in previous works [32–34]. Briefly, a pulsed Nd:YAG laser (Quantel Brilliant b, 6 ns, 1064 nm, 850 mJ) was focused just below the thin residue sample surface, forming a high-temperature ( $> 10,000$  K) microplasma that lasts for tens of microseconds, initiating exothermic chemical reactions of the ablated materials in the plasma. The initiated exothermic reaction further accelerates the laser-induced shock wave and the expansion of the shock wave into the air above the sample was recorded with a typical Z-type schlieren imaging setup using a high-speed color camera at 84,000 fps (1  $\mu\text{s}$  shutter). The positions of the laser-induced shock waves as a function of time were measured to determine the characteristic laser-induced shock velocity of each sample.

## 3. Results and discussion

### 3.1. Material characterization of perfluoroalkyl-functionalized nAl particles

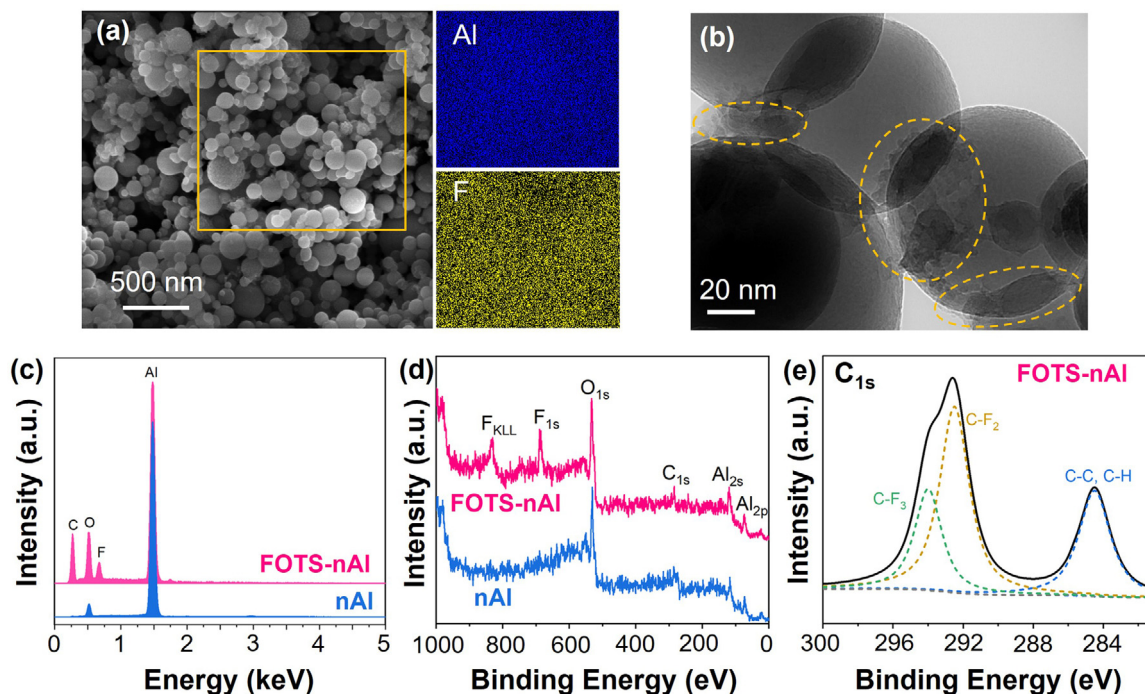
Figure 2 shows the morphology, chemical composition, and surface states of the perfluoroalkyl-functionalized nAl particles. The spherical shape and smooth surface morphology of the pristine nAl particles are preserved after surface functionalization (Fig. 2a and Fig. S1). The SEM/EDS mapping shows consistent distributions of Al and F elements, implying that a thin layer of perfluoroalkylsilane is present on the nAl surface. The functionalization layer is

also observed by SEM/EDS mapping of the much larger  $\mu\text{Al}$  particles, which shows the presence of fluorine on the surface of particles (Fig. S2). The TEM image shows that the surface of FOTS-nAl is covered by a thin amorphous layer (Fig. 2b) with additional sporadic  $\gamma\text{-Al}_2\text{O}_3$  deposits [35], as specified by the orange circled regions and the EDS spectrum shows that the fluorine content is about 6.2 at.% and the mass percentage of the perfluoroalkylsilane in FOTS-nAl is about 7.5 wt%. The XPS analysis (Fig. 2d and 2e) also confirms the existence of fluorine and the existence of C-F<sub>2</sub> and C-F<sub>3</sub> groups on the nAl surface.

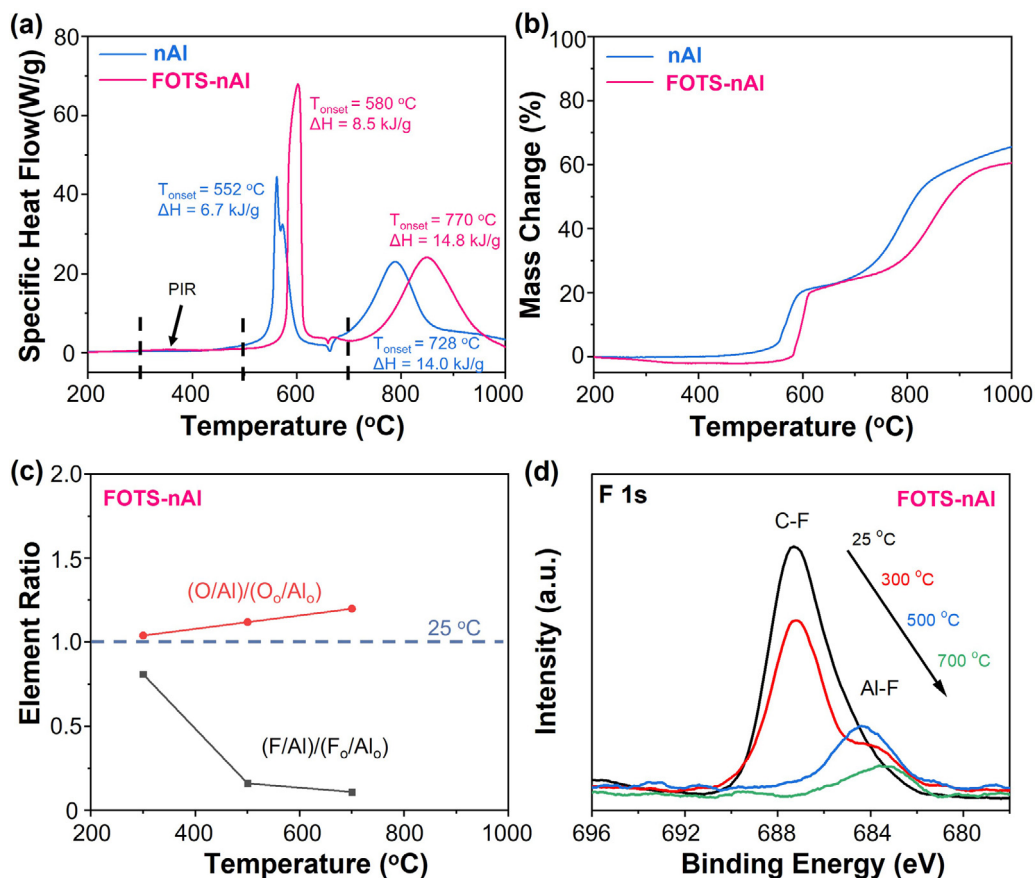
### 3.2. Ignition and thermochemical behaviors at a slow heating rate

Figure 3a and 3b compare the measured specific heat flow and mass change of nAl and FOTS-nAl in air measured by TGA/DSC (heating rate: 10 °C/min). First, both particles show similar behaviors, one small endothermic peak at 660 °C (melting of Al) and two large exothermic peaks accompanied by a large mass increase, which should correspond to the oxidation of Al. The existence of two large exothermic peaks is likely caused by the size nonuniformity of nAl particles and incomplete oxidation in the solid phase (before the melting of Al). Secondly, the onset temperatures of the two exothermic peaks for FOTS-nAl particles are about 30–50 °C higher than those of pristine nAl particles. The first delayed onset of the functionalized nAl particles can be attributed to the relatively thicker Al surface shell from the products of the perfluoroalkylsilane decomposition. The delayed onset for the oxidation peak after Al melting is caused by a higher content of solid-phase Al<sub>2</sub>O<sub>3</sub> in the FOTS-nAl sample as a higher degree of Al is oxidized before the Al melting. Thirdly, the FOTS-nAl sample exhibits a  $\sim 2\%$  mass drop at 300–400 °C with a tiny exothermic peak (Fig. S3 for a zoom-in plot), which can be attributed to the reaction between some decomposed fluorocarbons and Al<sub>2</sub>O<sub>3</sub>, known as the pre-ignition reaction (PIR) [22]. This also suggested that our functionalization layer is thin.

For FOTS-nAl particles, the resultant samples after heating to 300 °C (onset of PIR), 500 °C (end of PIR and before major oxidation), and 700 °C (after major oxidation) are analyzed via XPS to investigate further the changes in surface chemistry after each stage of heating. Figure 3c shows the O/Al and F/Al ratios estimated by XPS spectra for these temperatures normalized by their as-synthesized (25 °C) values. Figure 3d further shows the XPS F 1s peak evolution at those temperatures. It is interesting to note that some Al-F bonds are already formed at 300 °C, suggesting that some reaction between F and Al<sub>2</sub>O<sub>3</sub> has occurred at 300 °C [36]. The F/Al ratio in Fig. 3c shows a big drop around 300–500 °C after the PIR before the first major exothermic peak (Fig. 3a) and the surface chemical binding state of F shows a shift from C-F to Al-F bond. This confirms the decomposition of perfluoroalkyl molecules and PIR between the fluorocarbons and the native oxide layer (Fig. 3a and 3b). These findings suggest that during this slow heating condition, some perfluoroalkyl molecules evaporate or decompose, and others slowly react with the surface oxide to form the AlO<sub>x</sub>F<sub>y</sub> compounds on the surface [36]. A comparison between the O/Al and F/Al element ratios of 500 °C products of pristine nAl and FOTS-nAl (Table S1) also suggests that a thicker shell has formed on the Al surface in the FOTS-nAl sample. This thicker AlO<sub>x</sub>F<sub>y</sub> shell delays the first onset temperature of the oxidation of FOTS-nAl (Fig. 3a), leading to the enhanced thermal stability of functionalized nAl in comparison to the pristine-nAl, as suggested by previous works [26,28]. Furthermore, the Al-F peak decreases significantly from 500 to 700 °C (Fig. 3d) as oxyfluoride or fluoride becomes volatile. This opens up more channels for diffusion of Al and O, resulting in a higher heat release and mass increase during the solid-phase nAl oxidation (Fig. 3a and 3b).



**Fig. 2.** Materials characterization of the functionalized nAl (FOTS-nAl). Characterization on the as-prepared perfluoro-functionalized Al nanoparticles. (a) SEM and EDS elemental mapping of the FOTS-nAl particles, EDS mapping indicates the Al and F elements distribution in the orange rectangle; (b) TEM image of the FOTS-nAl particles; (c) EDS spectra of pristine nAl and FOTS-nAl particles; (d) XPS spectra of pristine nAl and FOTS-nAl particles; (e) XPS spectrum of C1s of FOTS-nAl particles, the peak deconvolution suggests the existence of fluorocarbon groups on nAl surface.



**Fig. 3.** Investigation of the ignition and combustion of perfluorocarbon-functionalized nAl at a slow heating rate (10 °C/min). (a) DSC and (b) TGA of pristine nAl and functionalized nAl (FOTS-nAl) in air. (c) Evolution of O and F element ratios of FOTS-nAl during slow heating. Al<sub>0</sub>, F<sub>0</sub>, and O<sub>0</sub> indicate the element ratios of the as-synthesized (25 °C) FOTS-nAl. The ratios were determined from the peak area in the XPS spectra of FOTS-nAl heated to different temperatures via TGA/DSC (as shown by the dashed lines in Fig. 3a). (d) XPS spectra of F1s of FOTS-nAl heated to different temperatures via TGA/DSC.

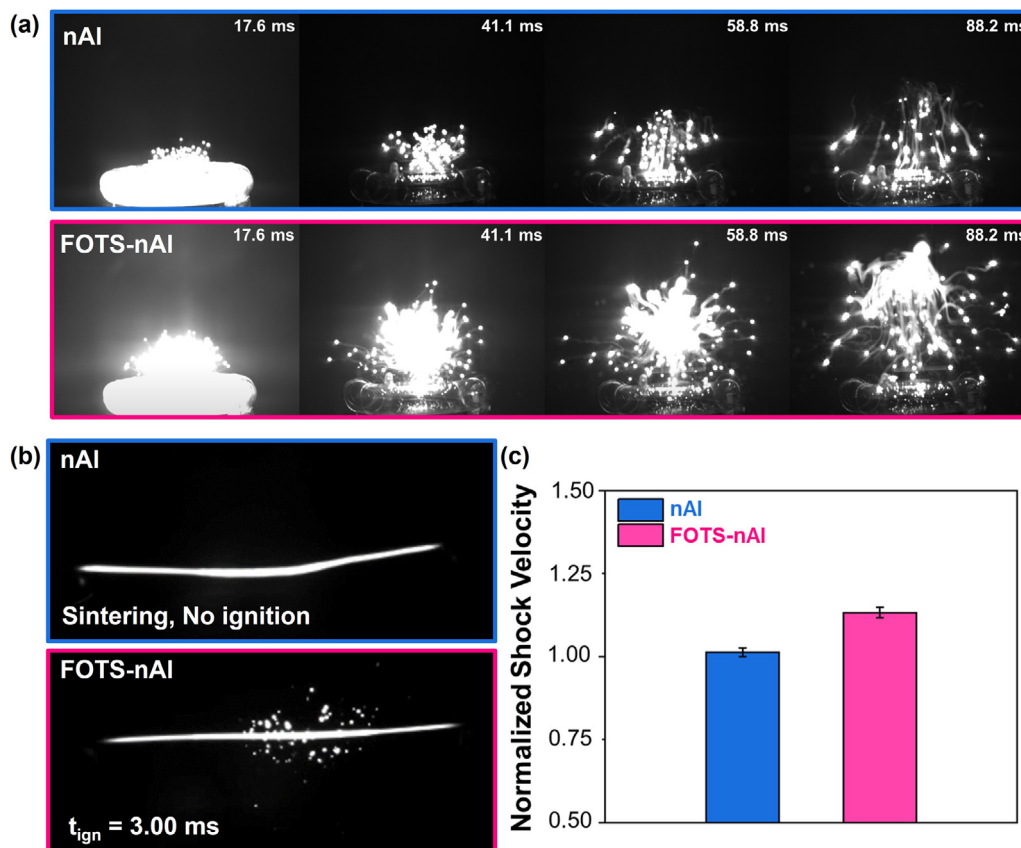


**Fig. 4.** Investigation of the ignition and combustion of perfluorocarbon-functionalized nAl at a fast heating rate. (a) ignition by Xe flash ( $2.1 \text{ J/cm}^2$ ,  $10^5$ – $10^6$  °C/s). Both samples can be ignited by the Xe flash but FOTS-nAl exhibits a more intense burning; (b) ignition by T-jump ( $10^5$ – $10^6$  °C/s) in air. Pristine nAl is not ignitable while FOTS-nAl exhibits an ignition delay time of 3 ms; (c) normalized laser-induced shock velocities measured by LASEM (up to  $10^{13}$  °C/s) for nAl and FOTS-nAl (normalized to the shock velocity of micron-sized Al).

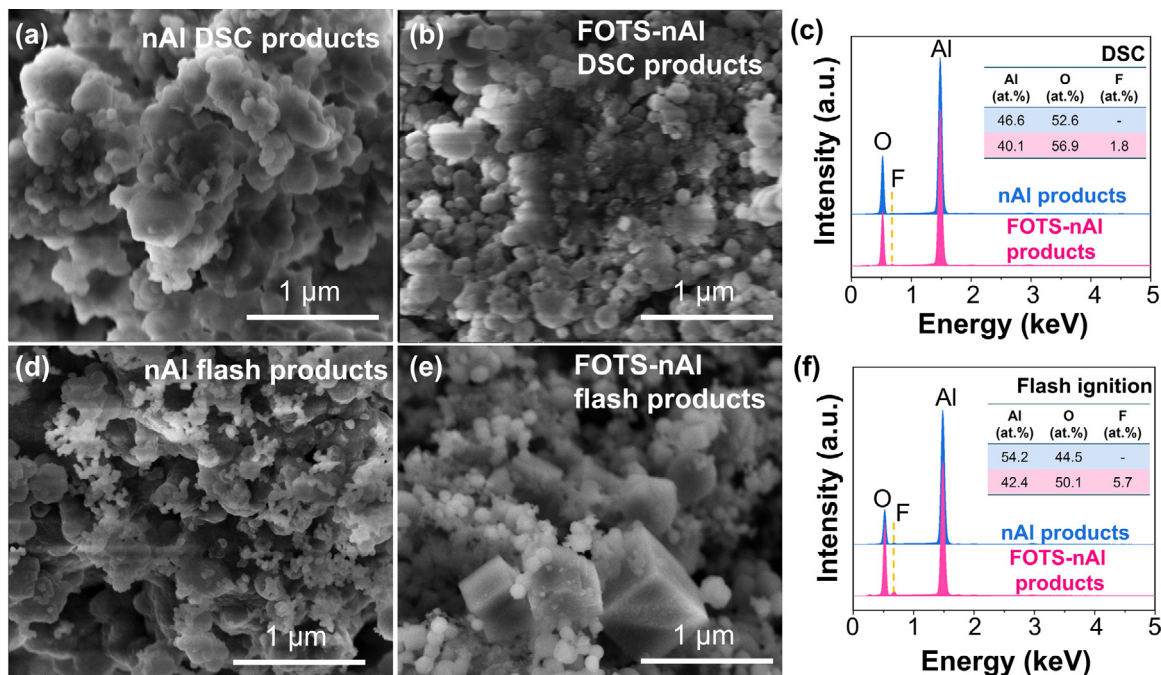


**Fig. 5.** Characterization of the combustion products of the pristine nAl and FOTS-nAl particles ignited under different heating conditions. (a) SEM of DSC products of nAl; (b) SEM of DSC products of FOTS-nAl; (c) EDS spectra of (a) and (b); (d) SEM of flash ignition products of nAl; (e) SEM of flash ignition products of FOTS-nAl; (f) EDS spectra of (d) and (e). For the nAl sample, it shows a higher extent of oxidation in DSC due to the slow heating condition. The FOTS-nAl sample has a higher oxidation degree in flash ignition, showing both higher O and F signals. The less F content in the DSC products of FOTS-nAl suggests that some fluorocarbons decompose at much lower temperatures and have limited reaction with nAl.

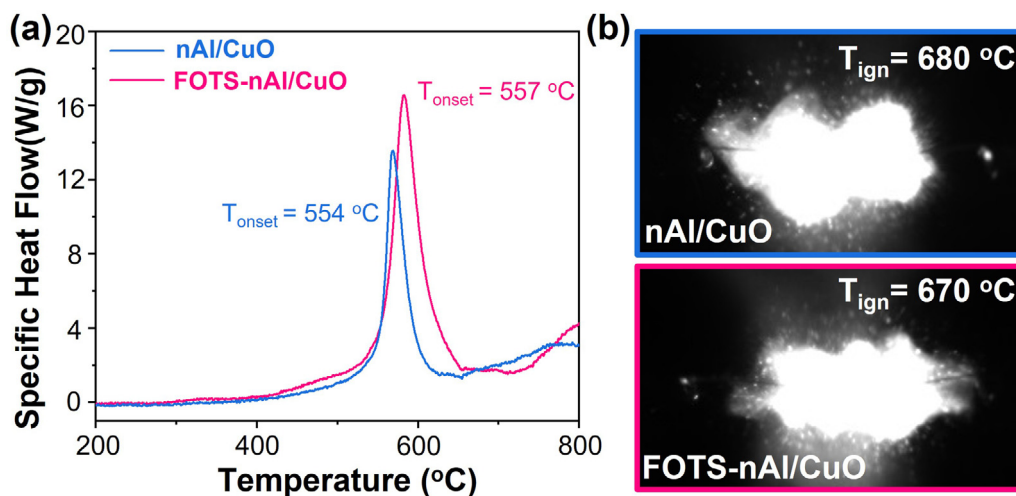


Fig. 6. Ignition of nAl/CuO thermite samples at (a) slow (DSC) and (b) fast (T-jump) heating rates.

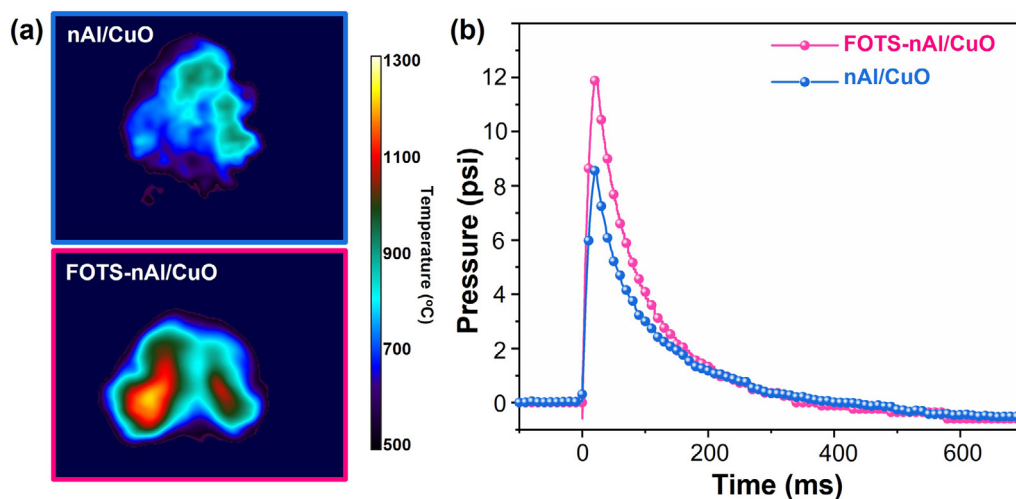


Fig. 7. Combustion of nAl/CuO thermite samples under fast heating conditions. (a) temperature measurement of the flash-ignited nanothermite by IR camera. The snapshots are obtained from the high-speed video taken by the IR camera and show the highest temperature achieved during the reaction of each sample. (b) time-resolved pressure evolution of the flash-ignited nanothermite in a constant-volume vial.

### 3.3. Ignition and burning properties at a fast heating rate

Figure 4 shows the ignition and combustion properties of the n-Al and FOTS-nAl with three fast heating rate methods: the Xe flash lamp ( $10^5$ – $10^6$  °C/s), T-Jump ( $10^5$ – $10^6$  °C/s), and LASEM technique ( $\sim 10^{13}$  °C/s). The Xe flash ignites both particles but the FOTS-nAl particles burn more violently with a larger burning footprint (Fig. 4a). The T-jump experiment shows that pristine n-Al particles only sinter without ignition (Fig. 4b) and the FOTS-nAl has an ignition delay time of 3.00 ms in air. At an even higher heating rate from LASEM (Fig. 4c), the FOTS-nAl also exhibits a higher laser-induced shock velocity ( $\sim 1.13$ , normalized to the velocity of micron-sized Al) [37] than the pristine nAl ( $\sim 1.01$ ), suggesting a higher microsecond-timescale energy release. Those results suggest that the localized fluorocarbon readily helps with the removal or break of the native oxide layer, which provides more reaction sites for Al oxidation and thereby promotes the ignition and burning (energy release) of nAl particles in the air [14]. On a separate note, the heat of combustion of the samples is compared in Fig. S4. It is found that FOTS-nAl exhibits a slightly higher combustion enthalpy due to the fluorination

of Al, and worth mentioning, better storage stability due to the hydrophobicity of the functionalized nAl surface.

### 3.4. Combustion products from different heating rates

The morphology and chemical composition of the combustion products are analyzed to further understand the effect of surface functionalization of nAl on the Al oxidation process under different heating conditions. As shown in Fig. 5a and 5b, the oxidation products of TGA/DSC consist of micron-sized clusters, indicating the anticipated sintering. The SEM/EDS spectrum in Fig. 5c also suggests that only 1.8 at.% of F remains in the products of FOTS-nAl after slow heating in TGA/DSC, which is obviously lower than the initial F content (6.6 at.%). In contrast, the combustion products from Xe flash ignition for FOTS-nAl and pristine nAl are significantly less sintered and contain many nanoparticles (Fig. 5d and 5e), similar to previous studies [38,39]. The product of FOTS-nAl also contains cubic  $\text{AlF}_3$  particles and the EDS spectra in Fig. 5f show that there is  $\sim 5.7$  at.% F left in the products. The difference in the remaining F contents of FOTS-nAl products from TGA/DSC and flash ignition further confirms that some fluorocarbons will decompose and

leave the surface of nAl under slow heating conditions, which is suppressed under fast heating conditions.

### 3.5. Effect of perfluoroalkyl-functionalization on ignition and combustion of nanothermite

After investigating the ignition and combustion behaviors of perfluoroalkyl-functionalized nAl particles, the effect of the perfluoroalkyl molecules is further studied in Al-based energetic materials. We chose Al/CuO nanothermite because it has been widely studied previously [40–43]. For TGA/DSC, perfluoroalkyl-functionalization has little effect on the onset temperature of the thermite reaction (Fig. 6a). For the T-jump ignition, the perfluoroalkyl-functionalized nanothermite and the pristine nanothermite have similar ignition temperatures (Fig. 6b), which is different from that of nAl particles (Fig. 4b). When the nanothermites are placed in a constant-volume vial and ignited by the Xe flash (Fig. 7), the FOTS-nAl/CuO shows a much higher peak temperature and peak pressure during the thermite reaction. These observations suggest that nAl/CuO already has good ignition properties due to the close contact between Al and CuO, so the additional fluorocarbon has little impact on its ignition. For combustion, the fluorine species actively reacts with Al<sub>2</sub>O<sub>3</sub> or Al, which provides extra combustion enthalpy besides the thermite reaction. A similar enhancement of fluorocarbon functionalization on thermite reaction is also observed for much larger  $\mu$ Al particles with CuO (Fig. S5), and interestingly it also reduces the ignition delay time of the  $\mu$ Al thermite by  $\sim$  10%.

## 4. Conclusions

In summary, this work studies the effect of perfluoroalkylsilane surface functionalization on the thermochemical and combustion behaviors of nAl particles under both slow and fast heating rates. Under the slow heating condition, part of the perfluoroalkylsilane molecules leave the nAl surface at low temperature without reaction, and the remaining perfluoroalkylsilane react with the surface oxide and form oxyfluoride compounds, improving the thermal stability of the nAl particles. In contrast, under fast heating conditions, the perfluoroalkylsilane molecules or their decomposed fluorine species have limited time to escape and actively participate in the ignition and combustion of nAl in air, leading to reduced ignition threshold and promoted oxidation. Similar enhancing effects were also observed for Al/CuO nanothermite under fast heating rates. These results indicate that surface functionalization with perfluoroalkylsilane can significantly improve the ignition and combustion properties of nAl particles. Because the decomposition temperature of perfluoroalkylsilane is lower than the oxidation onset temperature of nAl particles, their benefits are more pronounced when the reaction is initiated under fast heating conditions.

## Declaration of Competing Interest

The authors declare that they have no known competing financial interests or personal relationships that could have appeared to influence the work reported in this paper.

## Acknowledgement

This work was supported by the Office of Naval Research managed by Chad Stoltz under agreement number N00014-19-1-2085. University of California authors were supported by the Office of Naval Research.

## Supplementary materials

Supplementary material associated with this article can be found, in the online version, at doi:10.1016/j.combustflame.2022.112170.

## References

- [1] R.A. Yetter, Progress towards nanoengineered energetic materials, *Proc. Combust. Inst.* 38 (2021) 57–81.
- [2] V. Babuk, I. Dolotkazin, A. Gamsov, A. Glebov, L.T. DeLuca, L. Galfetti, Nanoaluminum as a solid propellant fuel, *J. Propuls. Power* 25 (2009) 482–489.
- [3] L.L. Wang, Z.A. Munir, Y.M. Maximov, Thermite reactions: their utilization in the synthesis and processing of materials, *J. Mater. Sci.* 28 (1993) 3693–3708.
- [4] H. Tyagi, P.E. Phelan, R. Prasher, R. Peck, T. Lee, J.R. Pacheco, P. Arentzen, Increased hot-plate ignition probability for nanoparticle-laden diesel fuel, *Nano Lett* 8 (2008) 1410–1416.
- [5] Y. Gan, L. Qiao, Combustion characteristics of fuel droplets with addition of nano and micron-sized aluminum particles, *Combust. Flame* 158 (2011) 354–368.
- [6] W. Pang, Y. Li, L.T. DeLuca, D. Liang, Z. Qin, X. Liu, H. Xu, X. Fan, Effect of metal nanopowders on the performance of solid rocket propellants: a review, *Nanomaterials* 11 (2021).
- [7] E.L. Dreizin, Metal-based reactive nanomaterials, *Prog. Energy Combust. Sci.* 35 (2009) 141–167.
- [8] Y. Huang, G.A. Risha, V. Yang, R.A. Yetter, Combustion of bimodal nano/micron-sized aluminum particle dust in air, *Proc. Combust. Inst.* 31 (2007) 2001–2009.
- [9] Y. Huang, G. Risha, V. Yang, R. Yetter, Analysis of nano-aluminum particle dust cloud combustion in different oxidizer environments, 43rd AIAA Aerospace Sciences Meeting and Exhibit, 2005.
- [10] D.S. Sundaram, V. Yang, V.E. Zarko, Combustion of nano aluminum particles (Review), *Combust. Explos. Shock Waves* 51 (2015) 173–196.
- [11] R.A. Yetter, G.A. Risha, S.F. Son, Metal particle combustion and nanotechnology, *Proc. Combust. Inst.* 32 (2009) 1819–1838.
- [12] Y. Jiang, S. Deng, S. Hong, S. Tiwari, H. Chen, K.-i. Nomura, R.K. Kalia, A. Nakano, P. Vashishta, M.R. Zachariah, X. Zheng, Synergistically chemical and thermal coupling between graphene oxide and graphene fluoride for enhancing aluminum combustion, *ACS Appl. Mater. Interfaces* 12 (2020) 7451–7458.
- [13] W. Wang, R. Clark, A. Nakano, R.K. Kalia, P. Vashishta, Effects of oxide-shell structures on the dynamics of oxidation of Al nanoparticles, *Appl. Phys. Lett.* 96 (2010) 181906.
- [14] J. Wang, Y. Qu, F. Gong, J. Shen, L. Zhang, A promising strategy to obtain high energy output and combustion properties by self-activation of nano-Al, *Combust. Flame* 204 (2019) 220–226.
- [15] E.R. Wainwright, T.P. Weihs, Microstructure and ignition mechanisms of reactive aluminum–zirconium ball milled composite metal powders as a function of particle size, *J. Mater. Sci.* 55 (2020) 14243–14263.
- [16] D.W. Kim, K.T. Kim, G.H. Kwon, K. Song, I. Son, Self-propagating heat synthetic reactivity of fine aluminum particles via spontaneously coated nickel layer, *Sci. Rep.* 9 (2019) 1033.
- [17] R.J. Jouet, A.D. Warren, D.M. Rosenberg, V.J. Bellitto, K. Park, M.R. Zachariah, Surface passivation of bare aluminum nanoparticles using perfluoroalkyl carboxylic acids, *Chem. Mater.* 17 (2005) 2987–2996.
- [18] D.A. Kaplowitz, G. Jian, K. Gaskell, A. Ponce, P. Shang, M.R. Zachariah, Aerosol synthesis and reactivity of thin oxide shell aluminum nanoparticles via fluorocarboxylic acid functional coating, *Part. Part. Syst. Charact.* 30 (2013) 881–887.
- [19] D.W. Kim, K.T. Kim, T.S. Min, K.J. Kim, S.H. Kim, Improved energetic-behaviors of spontaneously surface-mediated Al particles, *Sci. Rep.* 7 (2017) 4659.
- [20] Y. Jiang, A.R. Demko, J. Baek, X. Shi, L. Vallez, R. Ning, X. Zheng, Facilitating laser ignition and combustion of boron with a mixture of graphene oxide and graphite fluoride, *Appl. Energy Combust. Sci.* (2020) 100013 1–4.
- [21] K.W. Watson, M.L. Pantoya, V.I. Levitas, Fast reactions with nano- and micrometer aluminum: a study on oxidation versus fluorination, *Combust. Flame* 155 (2008) 619–634.
- [22] J. McCollum, M.L. Pantoya, S.T. Iacono, Activating aluminum reactivity with fluoropolymer coatings for improved energetic composite combustion, *ACS Appl. Mater. Interfaces* 7 (2015) 18742–18749.
- [23] S.K. Valluri, M. Schoenitz, E.L. Dreizin, Combustion of aluminum-metal fluoride reactive composites in different environments, *Propellants Explos. Pyrotech.* 44 (2019) 1327–1336.
- [24] H. Nie, S. Pisharath, H.H. Hng, Combustion of fluoropolymer coated Al and Al-Mg alloy powders, *Combust. Flame* 220 (2020) 394–406.
- [25] T.R. Sippel, S.F. Son, L.J. Groven, Aluminum agglomeration reduction in a composite propellant using tailored Al/PTFE particles, *Combust. Flame* 161 (2014) 311–321.
- [26] X. Ke, S. Guo, B. Gou, N. Wang, X. Zhou, L. Xiao, G. Hao, W. Jiang, Superhydrophobic fluorine-containing protective coating to endow Al nanoparticles with long-term storage stability and self-activation reaction capability, *Adv. Mater. Interfaces* 6 (2019) 1901025.
- [27] Z. Li, X. Zhao, G. Li, F. Gong, Y. Liu, Q. Yan, Z. Yang, F. Nie, Surface fluorination of n-Al particles with improved combustion performance and adjustable reaction kinetics, *Chem. Eng. J.* 425 (2021) 131619.

- [28] Y. Ou, Q. Jiao, N. Li, S. Yan, R. Yang, Pyrolysis of ammonium perfluorooctanoate (APFO) and its interaction with nano-aluminum, *Chem. Eng. J.* 403 (2021) 126367.
- [29] Y. Jiang, N.E. Dincer Yilmaz, K.P. Barker, J. Baek, Y. Xia, X. Zheng, Enhancing mechanical and combustion performance of boron/polymer composites via boron particle functionalization, *ACS Appl. Mater. Interfaces* 13 (2021) 28908–28915.
- [30] W. Zhou, J.B. DeLisio, X. Wang, M.R. Zachariah, Reaction mechanisms of potassium oxysalts based energetic composites, *Combust. Flame* 177 (2017) 1–9.
- [31] Y. Jiang, S. Deng, S. Hong, J. Zhao, S. Huang, C.-C. Wu, J.L. Gottfried, K.-i. Nomura, Y. Li, S. Tiwari, R.K. Kalia, P. Vashishta, A. Nakano, X. Zheng, Energetic performance of optically activated aluminum/graphene oxide composites, *ACS Nano* 12 (2018) 11366–11375.
- [32] J.L. Gottfried, E.R. Wainwright, S. Huang, Y. Jiang, X. Zheng, Probing boron thermite energy release at rapid heating rates, *Combust. Flame* 231 (2021) 111491.
- [33] E.R. Wainwright, S.W. Dean, S.V. Lakshman, T.P. Weihs, J.L. Gottfried, Evaluating compositional effects on the laser-induced combustion and shock velocities of Al/Zr-based composite fuels, *Combust. Flame* 213 (2020) 357–368.
- [34] J.L. Gottfried, Influence of exothermic chemical reactions on laser-induced shock waves, *Phys. Chem. Chem. Phys.* 16 (2014) 21452–21466.
- [35] C.-C. Wu, J. Wen, S.D. Walck, R.A. Pesce-Rodriguez, I. Arslan, Advanced nanoscale characterization of aluminum nanoparticles with modified surface morphology via atmospheric helium and carbon monoxide plasmas, *J. Appl. Phys.* 129 (2021) 063302.
- [36] P.J. Chen, R.M. Wallace, S.A. Henck, Thermal properties of perfluorinated n-alkanoic acids self-assembled on native aluminum oxide surfaces, *J. Vac. Sci. Technol. A* 16 (1998) 700–706.
- [37] J.L. Gottfried, S.W. Dean, C.-C. Wu, F.C. De Lucia, Measuring fast and slow energy release from aluminum powders, *AIP Conf. Proc.* (2020) 060016 2272.
- [38] Y. Ohkura, P.M. Rao, X. Zheng, Flash ignition of Al nanoparticles: mechanism and applications, *Combust. Flame* 158 (2011) 2544–2548.
- [39] W. Wang, R. Clark, A. Nakano, R.K. Kalia, P. Vashishta, Fast reaction mechanism of a core(Al)-shell (Al<sub>2</sub>O<sub>3</sub>) nanoparticle in oxygen, *Appl. Phys. Lett.* 95 (2009) 261901.
- [40] S. Deng, Y. Jiang, S. Huang, X. Shi, J. Zhao, X. Zheng, Tuning the morphological, ignition and combustion properties of micron-Al/CuO thermites through different synthesis approaches, *Combust. Flame* 195 (2018) 303–310.
- [41] M. Weismiller, J. Malchi, R. Yetter, T. Foley, Dependence of flame propagation on pressure and pressurizing gas for an Al/CuO nanoscale thermite, *Proc. Combust. Inst.* 32 (2009) 1895–1903.
- [42] G. Jian, N.W. Piekielek, M.R. Zachariah, Time-resolved mass spectrometry of nano-Al and nano-Al/CuO thermite under rapid heating: a mechanistic study, *J. Phys. Chem. C* 116 (2012) 26881–26887.
- [43] H. Wang, D.J. Kline, P. Biswas, M.R. Zachariah, Connecting agglomeration and burn rate in a thermite reaction: role of oxidizer morphology, *Combust. Flame* 231 (2021) 111492.